10th International Conference on Contact Mechanics
CM2015, Colorado Springs, Colorado, USA

Computation of the flash-temperature at the wheel-rail contact using a 3D finite element model and its comparison with analytical methods

M. Naeimi[1], Z. Li[1], R. Dollevoet[1], J. Wu[2], R. H. Petrov[2,3], J. Sietsma[2,3]

[1] Section of Railway Engineering, Faculty of Civil Engineering and Geoscience, Delft University of Technology, Delft, the Netherlands
[2] Department of Materials Science and Engineering, Delft University of Technology, Delft, the Netherlands
[3] Department of Materials Science and Engineering, Ghent University, Ghent, Belgium

ABSTRACT
The coupled mechanical–thermal behaviour of wheel and rail materials under rolling contact is studied to determine the temperature rise due to the frictional heat. The wheel–rail frictional rolling contact problem is solved using the three–dimensional finite element (FE) method. The FE model considers the wheel tread–rail top contact with partial-slip and converts the frictional energy into the heat as an attempt to estimate the temperature rise. Instead of assuming a global sliding velocity (a conventional premise in the field), the relative velocities of wheel-rail nodes in the contact patch are automatically taken into account in the coupled analysis (instantaneous micro-slip in contact points). Different levels of traction forces are studied which determine the amounts of frictional energy. The thermal properties are specified for the materials. Defining the contact regions of the wheel and rail as the thermal conduction boundary conditions, the frictional energy is converted into heat within the contact interface. After generating the energy flux, the heat conduction occurs in three dimensions both in the wheel and rail. A steady state implicit analysis is considered for the thermal solver, whereas the mechanical solver benefits from an explicit solution scheme. Distributions of stresses and temperatures in the contact patch are made available by analysing various loading conditions. Considering the formulations offered by three analytical methods in the literature, the results of rail temperature i.e. longitudinal distributions and peak values are calculated. Though they are much more simplified problems, these analytical methods are considered as the reference models (benchmark) for comparison. The same input data are used for all the reference models to enable the comparison. The outputs of numerical simulations are compared with the reference data, with discussion on similarities and discrepancies. The proposed model is able to calculate the flash-temperature in wheel and rail materials by dropping some of the conventional assumptions used in the analytical approaches.
Key words: Flash-temperature, frictional heat, wheel–rail contact, finite element method

1 Introduction

Heat generation due to friction at the contact surfaces between wheel and rail is a common problem in railway engineering. The resulting thermal effects may cause material phase change and formation of the so–called white etching layer (WEL) under certain conditions. WEL is supposed to play an important role in the development of rolling contact fatigue.

Determination of temperature at the wheel–rail contact interface has been an ongoing research for many years. A fully analytical solution of the temperature field in sliding contact of the wheel-rail system was presented in [1]. Some other examples of analytical approaches dealing with temperature effects can be found in [2, 3]. Due to the complexity of the coupled mechanical–thermal behaviour, numerical approaches were used more frequently. [4-8] are some examples of using finite element analysis (FEA) for investigating the frictional heat generation and temperature rise in contact bodies. Besides the studies on thermal behaviour of the frictional contact, extensive research has also been carried out on mechanical aspects of the wheel–rail contact, see e.g. [9-11]. Using FE analysis, some studies [12-15] have investigated the coupled effects of the mechanical and thermal aspects. However, much simplification still exists in such mixed approaches; since they are mainly developed based on the 2D contact problem. Apart from a recent research [16], there is a general lack of the mechanical-thermal analysis in three dimensions. Although the numerical model of [16] benefits from a 3D FE modelling, the thermal calculation is performed separately from the mechanical simulation (uncoupled analysis). In this paper, however, a 3D FE model of the wheel–rail contact is built based on a synchronic thermo-mechanical approach. The model uses a transient explicit solver and it is capable of estimating temperature rise in wheel-rail materials. In the mechanical part, the 3D transient FE model is able to solve both the normal and the tangential contact problems simultaneously for arbitrary wheel-rail geometries. In the thermal part, a steady state implicit analysis is used which is coupled with the mechanical solver.

2 Analytical methods for calculating the flash-temperature

[17, 18] are examples of fundamental works on flash-temperature concept. In a number of studies, see [19, 20] for example, analytical methods were used for estimation of frictional heat and temperature rise. The contact temperature was analytically studied in [21], for the cases of constant and elliptical heat flows due to friction in the wheel-rail contact. A survey of various methods for the calculation of temperature in wheel-rail contact was offered by [22]. It compared analytical and numerical methods. These two works ([21, 22]) together with [23] are considered in this paper as the references; their results are compared with the those of a 3D FE model to be proposed in this paper. It is noteworthy to mention that [21, 22] used the same 2D analytical formulation for derivation of the heat equations whereas, the difference was in the methods applied to solve the equations. Another difference was that [21] used a 2D contact mechanics solution whereas [22] employed the a kind of approximation for the 3D Hertzian solution. The elliptical contact patch of [22] is divided into rectangular strips parallel to the rolling direction and the temperature field within the strips was calculated using the 2D heat equation. Formulation of the rolling contact problem involving frictional heat in [23] is a 2D approach, but more general, namely, heating occurred only in the slip zone. This work used Green functions to reduce the problem into a nonlinear system of integral equations which was numerically solved. It should be noted that some references, e.g. [22, 23], used analytical methods as the basis of temperature calculations, while they applied kind of numerical methods for calculating the final equations. All these methods are called as analytical methods in this paper. A brief description of the approach of [21, 22] is given in the following.

A particle in the rail surface is in contact with the wheel during a very short period. For calculation of the flash-temperature due to frictional heat, a very thin layer in the rail surface can be considered as the instantaneous affected zone. The thermal penetration depth in rail can be related to semi-axis of the contact patch a and the non-dimensional Péclet number P_e [22]:

$$\delta = \frac{a}{\sqrt{P_e}} \tag{1}$$

The Péclet number can be related to the forward velocity V_0 (vehicle speed) and the thermal diffusivity κ. The effect of material properties is introduced by thermal diffusivity, which combines thermal conductivity λ, density ρ and specific heat capacity c:

$$P_e = \frac{aV_0}{2\kappa} \quad , \quad \kappa = \frac{\lambda}{\rho c} \tag{2}$$

According to [21], if $P_e > 10$, the heat conduction occurs only perpendicular to the contact plane, i.e. in the vertical direction (z). This condition is basically valid for typical situations of the wheel-rail system. Therefore, the longitudinal (x) and lateral (y) heat conduction can be neglected. The heat conduction equation in z-direction (rail depth) can be written by:

$$\kappa \frac{\partial^2 T}{\partial z^2} = \frac{\partial T}{\partial t} \tag{3}$$

which is a second-order partial deferential equation involving temperature rates of change with respect to the time and rail depth. The material particles in the contact patch are subjected to the frictional heat source $\dot{q}(t)$, while the wheel is passing the rail. Assuming zero temperature as the initial state, the boundary condition at time t can be written as:

$$\lambda \frac{\partial T}{\partial z}(z = 0, t) = \dot{q}(t) \tag{4}$$

The time parameter (t) can be substituted by the wheel position in longitudinal direction (x) using $x = \mathrm{V}t$. Therefore, the heat conduction equation (only in z direction) will include the wheel sweeping on rail in the longitudinal direction. The dimensionless coordinates of each material particle in rail (2D) can be represented by:

$$\xi = \frac{x}{a} \quad , \quad \zeta = \frac{z}{\delta} \tag{5}$$

Defining β as the thermal penetration coefficient and V_w as the wheel velocity by the sum of the forward velocity V_0 and sliding velocity V_s:

$$\beta = \frac{\lambda}{\kappa}, \; V_w = V_0 + V_s \tag{6}$$

the general form of solution for the prescribed heat equation is written by [22]:

$$T_w(\xi, \zeta) = \frac{1}{\beta_w}\sqrt{\frac{a}{\pi V_w}}\int_{-1}^{\xi} \dot{q}_w(\xi') \times \exp\left(-\frac{\zeta^2}{2(\xi - \xi')}\right)\frac{d\xi'}{\sqrt{\xi - \xi'}} \tag{7}$$

$$T_r(\xi, \zeta) = \frac{1}{\beta_r}\sqrt{\frac{a}{\pi V_r}}\int_{-1}^{\xi} \dot{q}_r(\xi') \times \exp\left(-\frac{\zeta^2}{2(\xi - \xi')}\right)\frac{d\xi'}{\sqrt{\xi - \xi'}} \tag{8}$$

where subscripts w and r indicate the wheel and rail respectively. T_w and T_w are temperatures of the wheel and rail respectively. This general solution includes solving the integral of the heat flow relative to the dimensionless ξ. The solution method is dependent upon the type of the heat flow function (polynomial, constant, elliptical or any other arbitrary function). For instance, it can be solved analytically for any distribution of heat flow rate given as a polynomial. An analytical approximation is proposed in [22] for the elliptical heat flow rate in the Hertzian contact:

$$\dot{q}_{friction}(\xi) = fV_s P_0 f(\xi), \quad f(\xi) = \frac{\pi}{2048}(645 - 210\xi^2 - 315\xi^4) \tag{9}$$

The temperature at the surface ($\zeta = 0$) in this method is calculated by:

$$T_{w/r}(\xi) = \frac{\varepsilon f V_s P_0}{\beta_{w/r}} \sqrt{\frac{a}{\pi V_{w/r}}} F(\xi) \qquad (10)$$

where $F(\xi)$ is calculated by different equations within or outside of the contact patch [22]:

$$for\ -1 < \xi < 1: \quad F(\xi) = \frac{\pi}{128}\left\{\sqrt{\xi+1}\times (71+12\xi-20\xi^2+8\xi^3-16\xi^4) - \sqrt{\xi-1}(71-12\xi-20\xi^2-8\xi^3-16\xi^4)\right\} \qquad (11)$$

$$for\ \xi > 1 or \xi < -1: \quad F(\xi) = \frac{\pi}{128}\sqrt{\xi+1}\times (71+12\xi-20\xi^2+8\xi^3-16\xi^4) \qquad (12)$$

According to [22], this approximation method is the best choice for the investigation of contact temperatures and thermal stresses in the case of the Hertzian contact.

Below the rail surface ($\zeta > 0$), the analytical formulation of the temperature based on constant heat flow rate $\dot{q}_{friction}$ is used in this paper. The reason is that, according to the results in [21, 22] the heat flow rate has mainly affected distributions of the temperature in the surface. Hence, the temperature in rail depth can be expressed as [22]:

$for\ -1 < \xi < 1$:

$$T_{w/r}(\xi,\zeta) = \frac{\dot{q}_{friction}}{\beta_{w/r}}\sqrt{\frac{2a}{V_w}}\left\{\sqrt{\frac{2(\xi+1)}{\pi}} \times \exp\left(-\frac{\zeta^2}{2(\xi+1)}\right) - \zeta\, erfc\left(\frac{\zeta}{\sqrt{2(\xi+1)}}\right)\right\} \qquad (13)$$

$for\ \xi > 1$:

$$T_{w/r}(\xi,\zeta) = \frac{\dot{q}_{friction}}{\beta_{w/r}}\sqrt{\frac{2a}{V_w}}\left\{\left[\sqrt{\frac{2(\xi+1)}{\pi}} \times \exp\left(-\frac{\zeta^2}{2(\xi+1)}\right) - \zeta\, erfc\left(\frac{\zeta}{\sqrt{2(\xi+1)}}\right)\right] - \left[\sqrt{\frac{2(\xi-1)}{\pi}}\exp\left(-\frac{\zeta^2}{2(\xi-1)}\right) - \zeta\, erfc\left(\frac{\zeta}{\sqrt{2(\xi-1)}}\right)\right]\right\} \qquad (14)$$

with the complement *erfc(x)* of the error function *erf (x)* defined by:

$$erfc(x) = 1 - erf(x) = 1 - \frac{2}{\sqrt{\pi}}\int_0^x e^{-\omega^2} d\omega \qquad (15)$$

This formulation is capable of calculating wheel and rail temperature for various distributions of frictional heat flow rate. Details of the mathematical approach for derivation of the prescribed equations can be found in [21, 22].

The formulations of [21, 22] for calculating temperature has been derived based on the following assumptions:

1) The wheel-rail contact occurs in two dimensions in steady state. Note that an approximate solution is proposed for the 3D problem in [22].
2) The heat conduction occurs only in one direction (perpendicular to the contact plane).
3) It is developed for the full-slip contact (there was a complete sliding).
4) The relative velocities of all the nodes in the contact patch are considered equal to the global sliding velocity.
5) The elliptical contact patch is considered for the wheel and rail with smooth geometries. Materials behave elastically according to the Hertzian theory.
6) The material properties and the coefficient of friction are considered independent of the temperature.
7) Heat losses due to radiation or convection are negligible.
8) The frictional work is converted completely into the heat. Dissipation by, for instance, wear is not considered.

Apart from assumptions 3 and 4, the rest of assumptions were also employed in [23]. Due to these limitations, analytical methods are not ideal techniques for the calculation of flash-temperature.

The temperature rise can be studied more accurately by the finite element method where most of the mentioned limitations can be dropped.

3 Temperature calculation in the 3D wheel-rail contact problem

Using finite element method, a numerical model is developed in this paper for the temperature calculation in a more realistic way. A 3D transient FE model is built to examine the coupled mechanical-thermal behaviour of the contact bodies with arbitrary geometries under frictional rolling contact.

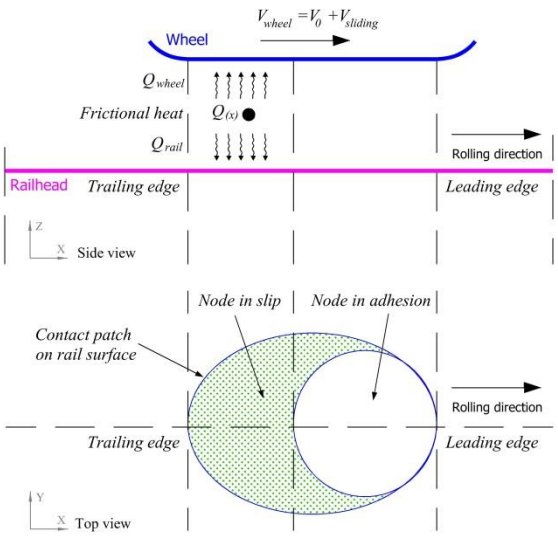

Fig. 1. Calculation of the temperature in partial-slip rolling contact, the side and top views are shown.

Among the above-mentioned assumptions which limit the applicability of the analytical methods, finite element method used in the current research is basically able to put down the assumptions 1-7. However, the FE model presented as the basic model in this paper drops only assumptions 1-4. Indeed, the temperature solution is sought for the 3D contact problem with partial slip using a transient time integration scheme. Fig. 1 shows this schematically. The heat flux is generated in the slip region only. Rolling contact with frictional heat generation is simulated with the wheel running with a constant speed on the rail.

3.1 Finite element modelling

Fig. 2 shows a schematic view of the 3D model. It includes a wheel, the primary suspension of the vehicle (spring-damper system) and a part of the railhead, resting on a rigid foundation. The components of the track such as railpads, sleepers, and ballast are not included; the quasi-static state of the contact problem is sought. The wheel and rail components are meshed with solid elements, having very fine mesh size in the running band (the finest mesh is around 0.6 mm).

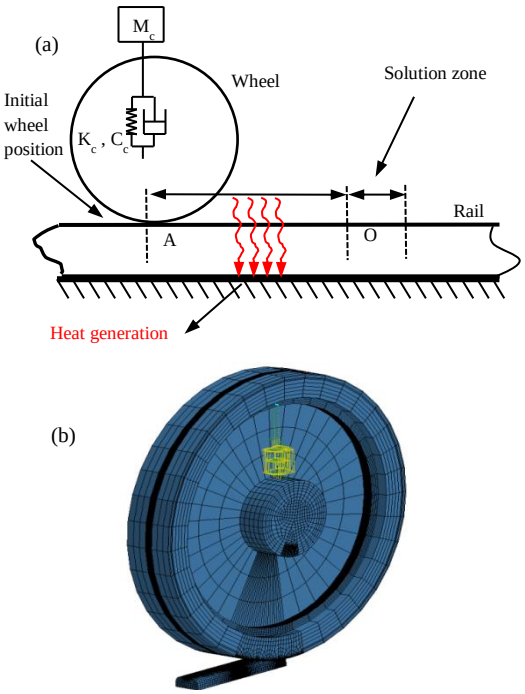

Fig. 2. The wheel–rail contact model (a) schematic view in the longitudinal–vertical direction, (b) the 3D view of the FE model

This model has originally been developed in [9] for the mechanical solution of the frictional rolling contact. The model is further advanced in the current research to deal with the thermo-mechanical problem. It simulates the wheel–rail contact with frictional heat generation during rolling. The material thermal structural response is simulated using finite element method capable of solving for the transient temperature under thermal/mechanical boundary conditions. A combined mechanical–thermal approach is used to estimate the flash–temperature at the wheel–rail interface; see Fig. 3. To perform the coupled analysis, the heat flux is firstly computed by the frictional contact (mechanical solver). Then, this is given as the input of thermal analysis for determining material thermal response. This leads to the distributions of stresses as well as temperature. Work done by friction can be transformed into deformation, wear and heat. In this paper, the effect of wear is assumed to be negligible, while deformations of materials under loadings are automatically considered during in the mechanical solution. By selecting appropriate timesteps for simulations, the mechanical and thermal solvers are connected in an iterative solution scheme. Using this coupled analysis the following advantages can specifically be outlined:

1) In the coupled analysis, material properties can be assumed to be temperature dependent. It should be noted that the results reported in the present paper are obtained for a simple case (temperature independent materials) to be comparable with the analytical methods.
2) As shown in Fig. 3, the geometries of the materials and the transient temperatures are spontaneously updated during the coupled simulation. Therefore, the effects of deformations and temperatures are interactively considered. This makes the model more accurate than using a thermal-only analysis under the presence of the heat flux.
3) The stresses are dependent on the temperature distribution in the frictional rolling contact. The coupled approach gives more realistic stress responses since the mechanical and thermal solutions are obtained simultaneously during the numerical simulation. It is noteworthy that in the current research neither the thermal properties nor the coefficient of thermal expansion are considered for the materials. Therefore, thermal stresses are negligible.

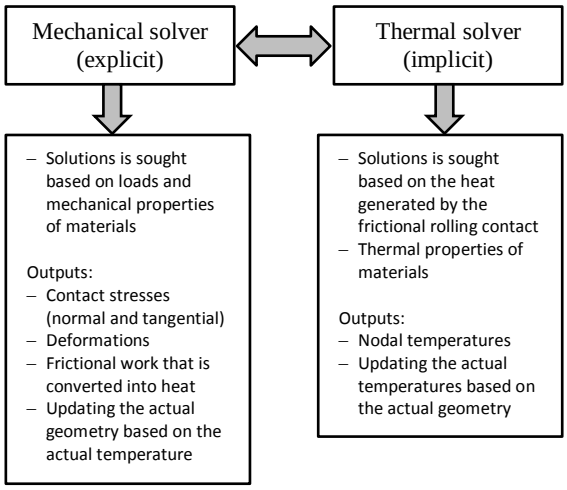

Fig. 3. The coupled mechanical-thermal analysis with the proposed FE tool

4 Input parameters

The loading data of the current study is taken from [9]. The thermal parameters of the coupled mechanical–thermal analysis are taken from [22]. The model parameters are listed in Table 1.

Various tangential loads (F) are simulated by applying different values of the traction coefficient on wheel (μ):

$$\mu = \frac{F}{N} \le f = 0.6 \qquad (16)$$

where, f denotes the friction coefficient. Four values of the traction coefficient i.e. 0.2, 0.3, 0.4 and 0.58 are considered to model different levels of partial slip. The greatest coefficient ($\mu=0.58$) simulates an almost full-slip contact.

Table 1. Reference parameters of the mechanical–thermal analysis

Symbol (units)	Description	Values
V_0 (m/s)	Forward velocity	38.889
s	Creepage (%)	0.27-1.2
V_s (m/s)	Sliding velocity (max.)	0.467
f	Coefficient of friction	0.6
μ	Traction coefficient	0.2-0.58
E (GPa)	Young's modulus of material	210
K_p (kN/m)	Stiffness of primary suspension	1150
C_p (Ns/m)	Damping of primary suspension	2500
υ	Poisson's ratio of material	0.3
κ (m^2/s)	Thermal diffusivity	1.518E-05
λ (W/Km)	Thermal conductivity	50
ρ (Kg/m^3)	Density of wheel-rail materials	7850
c (J/kg/°C)	Specific heat capacity	419.5
P_e	Péclet number	10258
N (kN)	Normal load	134
M_w (Kg)	Wheel weight	900
R_w (m)	Wheel radius	0.46

For the 3D model of the present research, only the longitudinal creepage is considered. The longitudinal creepage s is defined using the relative velocity between the two contact bodies:

$$s = \frac{V_{sliding}}{V_0} \qquad (17)$$

To relate the traction force to the creepage level, the Carter's equation is employed [24]:

$$s = \frac{fa}{R_w}\left(1-\sqrt{1-\frac{F}{fN}}\right) = -2\,fp_0E^*\left(1-\sqrt{1-\frac{F}{fN}}\right) \qquad (18)$$

in which, F and N are the tangential and normal contact force, respectively. R_w is the nominal rolling radius of the wheel and E^* is the elastic contact modulus which can be determined by:

$$E^* = \frac{1-\nu_1^2}{E_1} + \frac{1-\nu_2^2}{E_2} \qquad (19)$$

In this equation, wheel and rail materials have the Young's module of E_1 and E_2, while their Poisson's ratios are ν_1 and ν_2, respectively. When the level of creepapge is not too high (approximately less than 1%), the Carter's equation considers almost a linear relationship between the creepage and the creep force. For high creepages and for the full-slip contact a nonlinear relationship exists between the mentioned parameters, while the maximum creep force is limited to fN. By calculating creepages for different ratios of traction forces, the so-called creep curve in the present research is derived (Fig. 4).

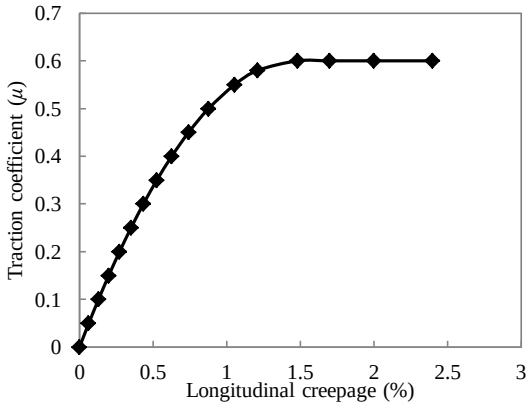

Fig. 4. The creep curve in the current study

5 Results and discussions

5.1 Stress analysis

The stresses in the rail material can be deduced from the FE model. Table 2 gives a summary of contact patch dimensions and stresses.

Table 2. A summary of contact patch dimensions and stresses

Symbol (units)	Description	Values
a (mm)	Semi-axis contact ellipse (longitudinal)	7.98
b (mm)	Semi-axis contact ellipse (lateral)	6.01
A (mm^2)	Contact patch area	150.4
p_0 (MPa)	Maximum vertical pressure	1352

By selecting a time-step during the simulation, 3D distributions of the pressure and surface shear stress were calculated. The results for the case $\mu=0.2$ are plotted in Fig. 5. The longitudinal and lateral axes on the rail surface were normalised relative to the semi-axes a and b, respectively. It should be noted that the wheel is located at $x=0$, while the leading edge and trailing edge of the contact patch are at $x=a$ and $x=-a$, respectively.

The longitudinal distributions of the pressure and tangential stress on the rail surface are demonstrated in Fig. 6 for various tractive efforts. As can be seen, the level of traction coefficient did not influence the pressure distributions significantly. On the contrary, the distribution and the peak magnitude of the surface shear stress were considerably dependent upon the amount of tangential load. The surface shear stress had a peak value occurring at the border of the slip and stick

regions followed by a decreasing trend toward the leading edge of the contact patch. With a high traction force (μ=*0.58*), distribution of surface shear stress tends to have an almost elliptical form.

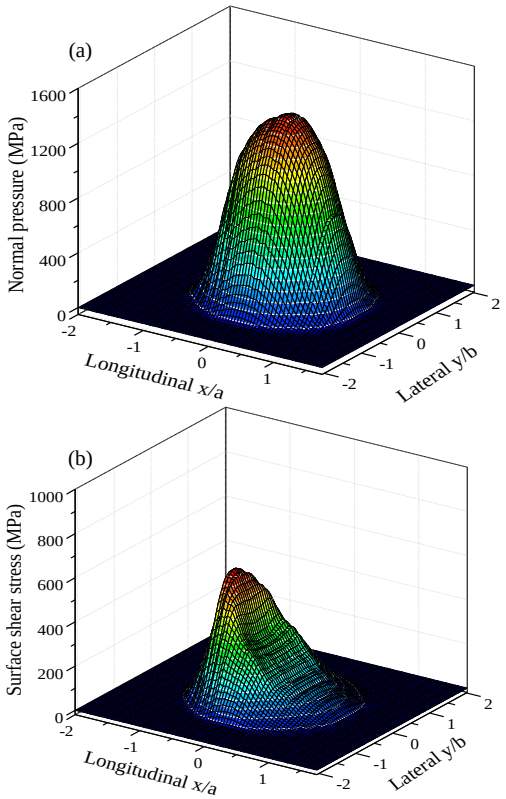

Fig. 5. 3D Distributions of (a) pressure and (b) shear stress in rail surface (μ=0.2)

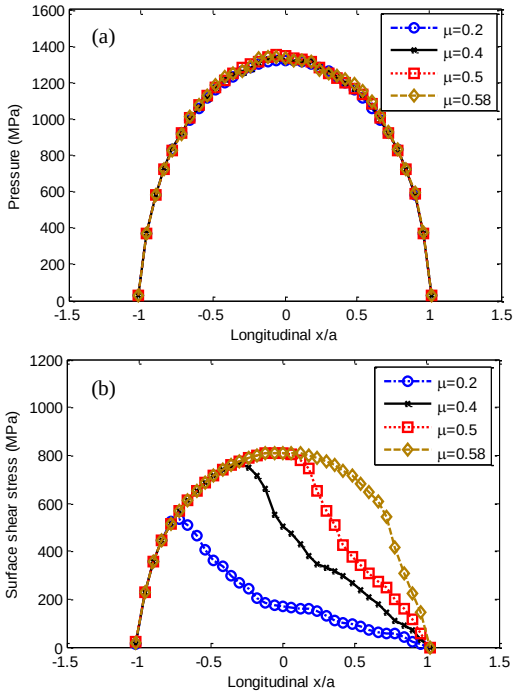

Fig. 6. 2D Distributions of (a) pressure and (b) shear stress in rail surface for different traction coefficients

The relative velocity of the contacting particles of the wheel and rail materials, i.e. the micro-slip in the contact patch is shown in Fig. 7. As is expected, the magnitude of the micro-slip decreased towards the leading edge of the contact patch in all the cases. The peak values of the micro-slip were obtained in the trailing edge of the contact patch. As the traction coefficient increased, greater magnitudes were recorded for the micro-slip.

Taking together, distributions of the pressure, surface shear stress and micro-slip in rail surface were in agreement with results of the mechanical model (only mechanical solver) in the former research [9]. Although the analysis type was different here (coupled analysis), because material properties were temperature independent with neglecting their thermal deformations, the same results were achieved.

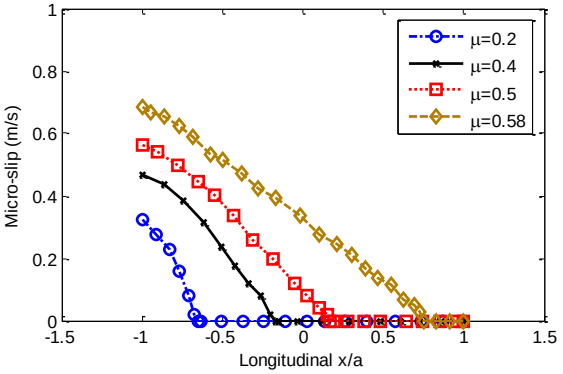

Fig. 7. Distributions of the micro-slip in rail surface (longitudinal) for various tangential loads

5.2 Rail flash-temperature

Results of temperature rise generated by frictional heat were deduced from the numerical simulation. A summary of the maximum flash-temperature for various traction coefficients are given in Table 3. Assuming zero temperature in the materials at the beginning of the simulations, the results are representative of the temperature rise generated by friction.

Table 3. A summary of the temperature rise in rail surface

Description	Values (*°C*)
Temperature rise (μ=*0.58*)	311
Temperature rise (μ=*0.50*)	213
Temperature rise (μ=*0.40*)	142
Temperature rise (μ=*0.20*)	50
Maximal temperature rise (peak μ)	311

According to Table 3, the peak temperature rise occurred in the FE model with the largest traction coefficient (μ=*0.58*). The 3D distributions of flash-temperature under different traction coefficients are shown in Fig. 8. The temperatures (vertical axes) were normalised relative to the maximum temperature in all plots.

Fig. 9 compares the longitudinal distribution of the contact temperature with the different tangential loads. Similar to the stress distributions, the abscissa of the figure is the distance along the rail,

which is normalised relative to the contact patch length.

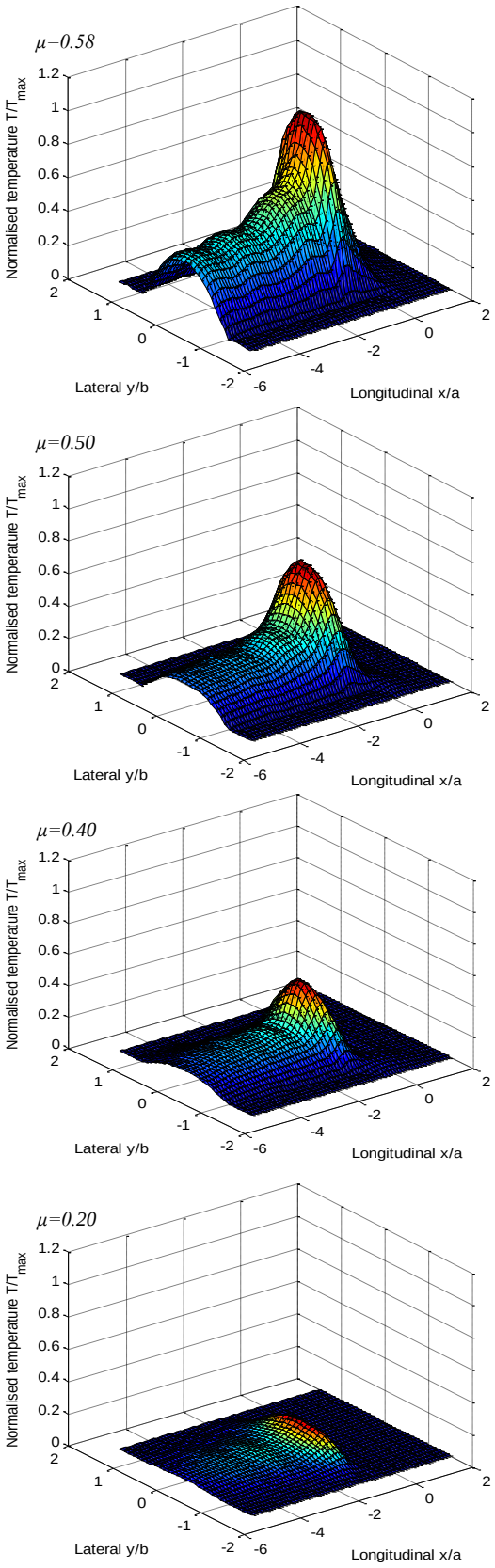

Fig. 8. 3D Distributions of temperature rise in rail surface for different tangential loads

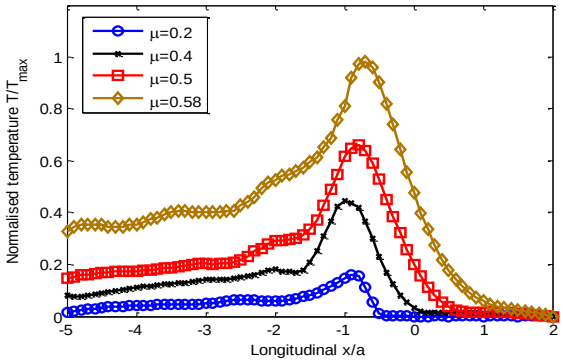

Fig. 9. 2D Distributions of temperature rise in rail surface, combined view of different cases

According to the results in Fig. 8-9, the following observations were made:

1) The distribution of the surface temperature had a peak occurred close to the trailing edge of the contact patch. The location of the peak temperature in longitudinal direction was around *-0.8a* (*x/a=-0.8)* for the largest μ. This was somewhat different for other loading cases. More precisely, temperature peaks occurred in a range of *-0.8a to -0.9a*.
2) As is expected, peak contact temperatures were significantly dependent on tangential loads. With larger traction coefficients, greater temperatures were produced. This is due to the fact that the micro-slip increased with higher tangential load. Indeed, the micro-slip occurring in the slip region of the contact patch generated the frictional heat. Therefore, both the peak temperature and the area of the heat generation region (slip zone) were increased by larger traction coefficients.
3) As is anticipated, the temperature rise for different cases reached to zero by approaching from peak temperature toward the leading edge of the contact patch (moving in rolling direction). At the leading edge of the contact, very small temperature was observed. An abrupt temperature decrease was seen moving from the peak value (near the trailing edge *0.8a to -0.9a*) to zero (variable location in the contact patch).
4) For smaller tangential loads, temperature came to zero before the leading edge. The zero limits were in the border of slip-adhesion regions; see Fig. 1. These findings agree with the fact that that the heat generation has occurred in the slip zone of the contact patch.
5) The contact temperature sharply decreased by moving away from the peak temperature toward the opposite direction of the rolling. The rate of temperature decay became slower after around *-1.5a*. The temperature rise with respect to the initial state could still be nontrivial even after *-5a*. The same tendency was found for different loading cases. This suggests that the contact temperature decayed slowly after *-1.5a* in the opposite direction of rolling.

5.3 Comparison with analytical solutions

According to formulations of the analytical solutions proposed by Knothe and Liebelt [21], Ertz and Knothe [22] and Pauk and Zastrau [23], distributions and maximum contact temperatures in the rail surface were calculated. It should be noted that [21] considered a numerical method for solving the equation with an arbitrarily-distributed heat source. The second benchmark [22] proposed an improved efficient approximation for the same problem of [21]. The last benchmark model [23] used a numerical procedure for solving the thermal equations.

To enable a comparison, the same parameters (Table 1) were considered for the different reference models. Moreover, a traction coefficient of $\mu=0.58$ is considered for all the cases. Based on Fig. 4, this value was considered as a full-slip contact. The maximum temperature in all the models occurred in the full-slip condition, in which the micro-slip took place over almost the full length of the contact patch. Table 4 compares the results of the maximum surface temperature in the numerical simulation with those of the analytical solitons.

Table 4. Comparison of maximum surface temperatures in different methods

Method	Max. temperature (°C)	Location of max. temperature
Knothe & Liebelt, 1995[21]	285	*-0.65a*
Ertz & Knothe, 2002 [22]	287	*-0.64a*
Pauk & Zastrau, 2002 [23]	337	*-0.86a*
Numerical simulation	311	*-0.80a*

A comparison of temperature distributions by the different models is plotted in Fig. 10, in which the temperatures were normalised with the respective peak temperatures given in Table 4.

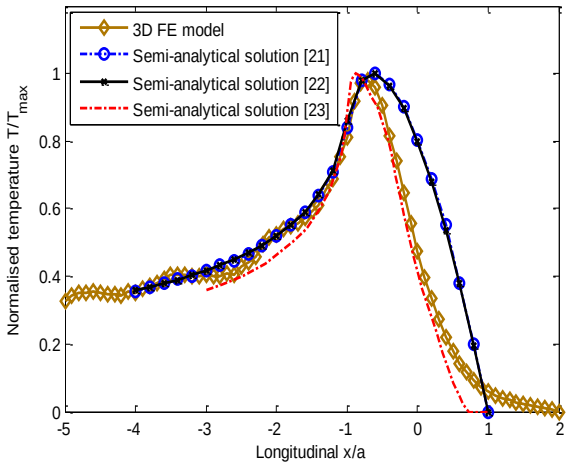

Fig. 10. Comparison of temperature distributions in different models

Looking at the results in Table 4 and Fig. 10, the following observations can be pointed out:

1) The maximum contact temperature of [21, 22] were almost equal to each other with the same distributions (local differences were less than 1%). In contrast, [23] produced a 18% higher temperature than the other two referenc with a somewhat different distribution. The peak surface temperature in the numerical simulation was between these two levels, while its distribution pattern was closer to [23]. The maximum contact temperature in the present research was around 8% higher than the results of [21, 22].
2) Comparing the temperature distributions of the different models, one can see that the normalised temperature in the contact patch (from $x=-a$ to $x=a$) were more significant by [21, 22] than the numerical model. This was especially true in the interval $x=0$ to $x=a$.
3) The maximum contact temperatures in the different models occurred relatively close to the trailing edge of the contact patch. The numerical model of this study and the solution of [23] had temperature peaks closer to the trailing edge, i.e. *-0.80a* and *-0.86a*, respectively.

5.4 Thermal penetration depth

It is accepted by some researchers [19, 21, 22] that the high contact temperature only occurs in a very thin layer with the penetration depth up to $\delta=80\ \mu m$. To have an acceptable computation time (around 50h), the finest mesh in the numerical model was *0.6 mm*. This element size is far beyond the order of the penetration depth. Therefore, with the current mesh size it is not possible to properly track the distributions of temperature along rail depth. To have an estimation of the thermal penetration depth, the solutions of [21, 22] were sought. The calculation resulted in $\delta=78.9\ \mu m$ for both methods. The distribution of temperature below the rail surface is plotted in Fig. 11. The maximum temperature is at the surface, followed by a very sharp decrease along the depth. This suggests a high temperature gradient in the vertical direction.

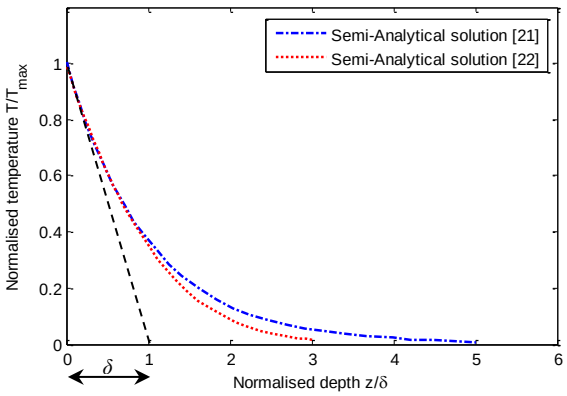

Fig. 11. Calculation of temperature in rail depth with analytical methods

5.5 The influence of creepage

As described before, a creepage-dependent distribution of tangential forces was used in the FE model of this research. Indeed, the numerical model

considered the creepage as function of the traction force. The maximum traction coefficient (μ=0.58), simulating almost the full-slip contact, led to 1.2% longitudinal creepage. Previous studies [8, 16, 22] suggested that the temperature rapidly increases with growing creepage. This was also confirmed by the current research for the creepage levels up to 1.2%. Increasing creepage beyond this level was not still accessible within the current model. The reason is that the traction force was directly applied on the wheel in the FE model instead of creepage. To assess the effect of creepages higher than 1.2% on surface temperature, a linear relationship based on [8, 22] is used. These references linearly relate the heat flux (and as a result the temperature) to the creepage. The results of the maximum surface temperature with increasing creepage parameter are plotted in Fig. 12.

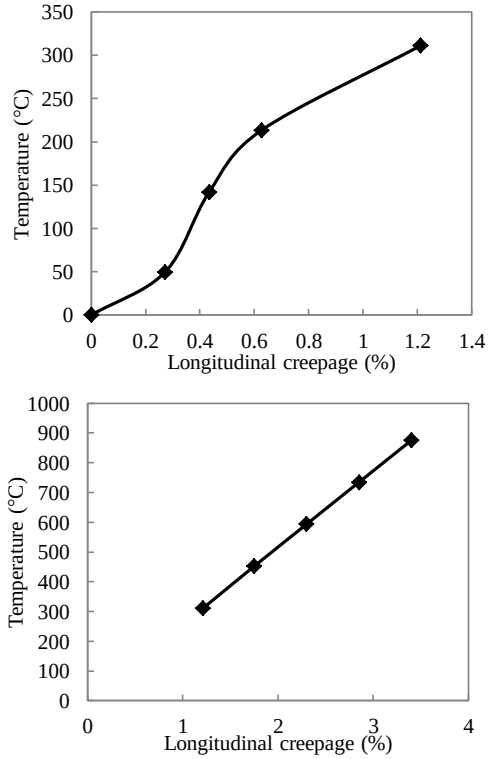

Fig. 12. Maximum temperatures of the rail surface for different longitudinal creepages, (a) results of numerical simulations for creepages up to 1.2%, (b) linear approximation for higher creepages

As shown in Fig. 12, the results of surface temperature were substantially dependent of the creepage level. Although the maximum temperature within the numerical simulation was only 311°C for the 1.2% creepage, the temperature rise due to high creepage can be as high as 900 °C, see Fig. 12(b).

5.6 The possibility of material phase change

According to [21, 25], a temperature of at least 600 °C would be needed to induce phase transformation in wheel and rail materials. With assumptions of the current research, a creepage of around 2.4% would be necessary to acquire the temperature rise of 600 °C in the rail surface. As a matter of fact, creepage levels higher than 1.2% are likely to happen in railways, particularly in locations with high tractive/braking efforts. Therefore, the creepage seem to be a potential parameter to increase the contact temperature.

Besides creepage, other parameters of the vehicle-track system (see Table 1), can influence the maximum temperature. Among various parameters, the normal load, coefficient of friction and vehicle speed are more crucial. Increasing these parameters leads to higher contact temperature. There are often uncertainties with the input parameters, particularly with regard to the coefficient of friction. Due to this fact, relatively large values were employed for the parameters in this research to come up with the extreme conditions.

6 Conclusions

A numerical model was developed in the present research to determine the flash-temperature in the rail material, within a coupled mechanical–thermal process. The main advantage of the FE model for temperature calculation was that it dealt with the wheel-rail contact problem in three dimensions, as well as considering frictional rolling contact and partial slip. Results of numerical simulations were compared with the reference outputs of three analytical solutions in the literature. The following conclusions can be drawn from the results and discussions:

1) Distributions of the pressure, surface shear stress and micro-slip in rail surface were in agreement with results of the former gross-mechanical model in the literature. This was likely to happen, since the temperature-dependent material properties were not considered in this paper. As expected, the peak shear stress and micro-slip were considerably dependent upon the amount of tangential load.
2) Under the assumptions used in the present research, the results of numerical model were consistent with the data obtained in the benchmark methods. The maximum surface temperature was around 8% higher than two of the reference results, while it was 10% less than the third reference. High contact temperatures in different models occurred relatively close to the trailing edge of the contact patch. With the analytical methods one can quickly estimate the maximum flash-temperature in wheel-rail contact. On the other hand, the advantage of the proposed numerical model is that: 1) it would ends up with more realistic results for flash-temperature calculation, particularly in connection with arbitrary geometries of materials in contact, partial slip and instantaneous micro-slip of the contact points; 2) with the coupled mechanical-thermal analysis, the geometries of the materials and the transient temperatures are spontaneously updated during the coupled simulation; 3) the stresses are dependent on the temperature leading to more realistic stress responses; 4) it can be further advanced for more complex

problems e.g. considering temperature dependency in material properties and friction coefficient.

3) With nominal parameters of the railway system, the maximum rail temperature was estimated only around 311°C with a longitudinal creepage of 1.2%. As expected, increasing creepage caused a steep growth in temperature. With a creepage of around 2.4% it was possible to achieve a temperature rise up to around 600 °C in the rail surface. The high temperatures can only occur when the level of creepage goes beyond the full-slip contact. Although a creepage of 1.2% (with a corresponding friction coefficient of 0.6) was considered as a threshold for the full-slip condition, higher creepage was needed to increase the heat flux and as a consequence, the contact temperature. Indeed, the maximum traction coefficient (0.58) only induced a temperature rise of 311°C, while with a high creepage of around 2.4%, temperature exceeded 600 °C.
4) To come up with the extreme conditions, relatively large values were employed for the normal load, coefficient of friction and vehicle speed. Among other factors, the creepage seemed to be the most potential parameter to increase the contact temperature.

The most likely consequence of high temperatures in wheel and rail materials is the possibility of changing the steel structure. Future investigations will concentrate on calibration of the numerical model.

Acknowledgment

This research is part of an ExploRail project namely as Development of High–Performance Rail through Intelligent Metallurgy and Engineering (PRIME), in Delft University of Technology. This project (Code: 11247/ C38A07) is funded by Dutch rail infra manager ProRail and the Netherlands organization for scientific research (STW/NWO).

REFERENCES

[1] F.D. Fischer, E. Werner, W.Y. Yan, Thermal stresses for frictional contact in wheel-rail systems, Wear, 211 (1997) 156-163.

[2] F.D. Fischer, W. Daves, E.A. Werner, On the temperature in the wheel-rail rolling contact, Fatigue & Fracture of Engineering Materials & Structures, 26 (2003) 999-U991.

[3] V. Boucly, D. Nélias, S. Liu, Q.J. Wang, L.M. Keer, Contact analyses for bodies with frictional heating and plastic behavior, Journal of tribology, 127 (2005) 355-364.

[4] V. Gupta, G.T. Hahn, P.C. Bastias, C.A. Rubin, Calculations of the frictional heating of a locomotive wheel attending rolling plus sliding, Wear, 191 (1996) 237-241.

[5] A. Ovcharenko, M. Yang, K. Chun, F. Talke, Transient thermomechanical contact of an impacting sphere on a moving flat, Journal of Tribology, 133 (2011) 031404.

[6] J. Jergéus, Martensite formation and residual stresses around railway wheel flats, Proceedings of the Institution of Mechanical Engineers, Part C: Journal of Mechanical Engineering Science, 212 (1998) 69-79.

[7] L. Ramanan, R. Krishna Kumar, R. Sriraman, Thermo-mechanical finite element analysis of a rail wheel, International Journal of Mechanical Sciences, 41 (1999) 487-505.

[8] W. Li, Z. Wen, X. Jin, L. Wu, Numerical analysis of rolling-sliding contact with the frictional heat in rail, Chin J Mech Eng-En, 27 (2014) 41-49.

[9] X. Zhao, Z. Li, The solution of frictional wheel–rail rolling contact with a 3D transient finite element model: Validation and error analysis, Wear, 271 (2011) 444-452.

[10] K.D. Vo, A.K. Tieu, H.T. Zhu, P.B. Kosasih, A 3D dynamic model to investigate wheel–rail contact under high and low adhesion, International Journal of Mechanical Sciences, 85 (2014) 63-75.

[11] T. Telliskivi, U. Olofsson, Contact mechanics analysis of measured wheel-rail profiles using the finite element method, P I Mech Eng F-J Rai, 215 (2001) 65-72.

[12] A.M.S. Asih, K. Ding, A. Kapoor, Modelling rail wear transition and mechanism due to frictional heating, Wear, 284–285 (2012) 82-90.

[13] L. Wu, Z.F. Wen, W. Li, X.S. Jin, Thermo-elastic-plastic finite element analysis of wheel/rail sliding contact, Wear, 271 (2011) 437-443.

[14] T.C. Kennedy, C. Plengsaard, R.F. Harder, Transient heat partition factor for a sliding railcar wheel, Wear, 261 (2006) 932-936.

[15] I. Widiyarta, F. Franklin, A. Kapoor, Modelling thermal effects in ratcheting-led wear and rolling contact fatigue, Wear, 265 (2008) 1325-1331.

[16] K.D. Vo, A.K. Tieu, H.T. Zhu, P.B. Kosasih, A tool to estimate the wheel/rail contact and temperature rising under dry, wet and oily conditions, Computers in Railways XIV, (2014) 191-201.

[17] J.F. Archard, The temperature of rubbing surfaces, Wear, 2 (1959) 438-455.

[18] H. Blok, The flash temperature concept, Wear, 6 (1963) 483-494.

[19] M.A. Tanvir, Temperature Rise Due to Slip between Wheel and Rail - an Analytical Solution for Hertzian Contact, Wear, 61 (1980) 295-308.

[20] M. Ertz, K. Knothe, Influence of temperature and roughness on side friction between wheel and rail, Z Angew Math Mech, 81 (2001) S57-S60.

[21] K. Knothe, S. Liebelt, Determination of temperatures for sliding contact with applications for wheel rail systems, Wear, 189 (1995) 91-99.

[22] M. Ertz, K. Knothe, A comparison of analytical and numerical methods for the calculation of temperatures in wheel/rail contact, Wear, 253 (2002) 498-508.

[23] V. Pauk, B. Zastrau, 2D rolling contact problem involving frictional heating, International Journal of Mechanical Sciences, 44 (2002) 2573-2584.

[24] K.L. Johnson, Contact mechanics, Cambridge University Press, Cambridge, UK, 1987.

[25] G. Baumann, H. Fecht, S. Liebelt, Formation of white-etching layers on rail treads, Wear, 191 (1996) 133-140.